

Barrier distribution functions for the system ${}^6\text{Li} + {}^{64}\text{Ni}$ and the effect of channel couplingMd. Moin Shaikh,¹ Subinit Roy,^{1,*} S. Rajbanshi,¹ M. K. Pradhan,¹ A. Mukherjee,¹ P. Basu,¹ S. Pal,²
V. Nanal,² R. G. Pillay,² and A. Shrivastava³¹*Saha Institute of Nuclear Physics, 1/AF, Bidhan Nagar, Kolkata-700 064, India*²*Department of Nuclear and Atomic Physics, Tata Institute of Fundamental Research, Mumbai-400 005, India*³*Nuclear Physics Division, Bhabha Atomic Research Centre, Mumbai-400 085, India*

(Received 15 January 2015; revised manuscript received 12 February 2015; published 24 March 2015)

Background: The barrier distribution function is an important observable in low-energy nucleus-nucleus collisions because it carries the distinct signature of the channel-coupling effect that is dominant at low energies. It can be derived from the fusion excitation function as well as from the back-angle quasi-elastic excitation function. The barrier distribution functions derived from the two complimentary measurements, in general, appear to peak at an energy close to the Coulomb barrier for strongly bound systems. But for weakly bound projectiles, like ${}^6\text{Li}$, a relative shift is observed between the distributions.

Purpose: The present work investigates the barrier distribution functions from fusion as well as from the back-angle quasi-elastic excitation function for the ${}^6\text{Li} + {}^{64}\text{Ni}$ system. The purpose is to look for the existence of a shift, if any, between the two measured distribution functions, as reported for ${}^6\text{Li}$ collision with heavy targets. A detailed coupled-channel calculation to probe the behavior of the distribution functions and their relative shift has been attempted.

Measurement: A simultaneous measurement of fusion and back-angle quasi-elastic excitation functions for the system ${}^6\text{Li} + {}^{64}\text{Ni}$ was performed. The fusion excitation function was measured for the energy range of 11 to 28 MeV while the quasi-elastic excitation function measurement extended from 11 to 20 MeV. The barrier distribution functions were subsequently extracted from both the excitation functions and compared.

Results: A small shift of around 450 keV peak to peak is observed between the barrier distribution functions derived from the complementary measurements. Detailed coupled channel and coupled reaction channel calculations reproduced both the excitation functions and barrier distributions. The shift of about 550 keV resulted from the model predictions corroborate the experimentally observed value for ${}^6\text{Li} + {}^{64}\text{Ni}$ system.

Conclusions: The coupling to inelastic channels are found to be sufficient to describe the fusion-barrier distribution. The positive Q -value one-proton and one-neutron stripping channels, leading to three-body final states, on the other hand, play dominant roles in reproducing the barrier distribution from the back-angle quasi-elastic excitation function.

DOI: [10.1103/PhysRevC.91.034615](https://doi.org/10.1103/PhysRevC.91.034615)

PACS number(s): 25.70.Bc, 24.10.Eq

I. INTRODUCTION

The barrier distribution function [1–3] has evolved as an important tool to probe the reaction dynamics of nucleus-nucleus collision at energies around the Coulomb barrier of the colliding system. Heavy ion collisions in this energy regime are strongly influenced by the internal structure of the colliding nuclei. The coupling between the relative motion and the intrinsic degrees of freedom of the reactants such as the static deformations, collective excitations, nucleon or cluster transfers dominates the outcome of the collision process [4–9]. The interplay essentially modifies the effective interaction potential for collision and in turn splits the nominal Coulomb barrier into multiple barriers [5]. Consequently, the fusion of the colliding nuclei evolves from a one-dimensional to multidimensional barrier penetration process as the relative energy for collision approaches the barrier. The multidimensional barrier-penetration model explains the enhancement observed in the fusion cross section at energies below the barrier [3]. The *barrier distribution* function derived from the

measured fusion excitation function (D_{fus}), therefore, provides useful information regarding the effect of coupling between the channels and can be used to understand the consequence of these couplings on fusion reaction [10].

Barrier distribution can also be derived from the excitation function of the back-scattered quasi-elastic events, (D_{qel}) [2,11,12]. The alternative derivation of the distribution function from the back-angle quasi-elastic excitation function is possible because of the conservation of reaction flux in the collision process [2]. Barrier distributions obtained from two complementary experimental approaches are found to be similar for the systems where both the reactants are strongly bound [3,13]. The similarity of D_{fus} and D_{qel} occurs due to the dominance of fusion reaction in the absorption cross section at energies around the Coulomb barrier, which determines the reaction threshold for strongly bound systems. The question is if any other reaction process competes with or even dominates the fusion reaction in absorbing the flux at near or subbarrier energies, what happens to two barrier distributions? Zagrebaev [14] showed that for very heavy systems, where deep inelastic processes become important, the quasi-elastic barrier distribution represents the total reaction threshold distribution and it differs from the distribution derived from

*subinit.roy@saha.ac.in

fusion reaction. It was found that the peak of the quasi-elastic barrier distribution is located at a lower energy compared to that obtained from the fusion measurement [15,16].

The question becomes more pertinent when one of the colliding partners is weakly bound. Breakup or breakup-like processes, e.g., transfer followed by breakup, competes strongly with the fusion reaction in generating the absorption at low energies. Thus the investigation of barrier distributions derived from fusion and back-scattered quasi-elastic processes and their comparison becomes particularly interesting. Several studies of barrier distribution for systems with weakly bound projectiles have been carried out over the last decade [17–30]. Most of these studies involved extraction of barrier distributions either from the fusion or from the back-angle quasi-elastic excitation functions and subsequent analyses of the data within the framework of coupled-channel (CC) or continuum discretized coupled-channel (CDCC) models. A few of these works compared the distributions derived from the elastic cross sections and the fusion cross section [19,21,28]. The general observation is that the breakup of the projectile in the interaction field affects the quasi-elastic scattering to a greater extent and the barrier distribution derived from it is found to be broader than that derived from fusion [19]. Monteiro *et al.* [31], using the data of Refs. [22,32] for ${}^6\text{Li} + {}^{144}\text{Sm}$ system, showed that the peak of the distribution derived from the quasi-elastic back-scattering cross sections is shifted by about 1.5 MeV to lower energy compared to the peak of the fusion barrier distribution. It was argued that the shift occurred due to the presence of breakup-like processes at energies below the barrier. This corroborates the observation by Zagrebaev [14] for weakly bound systems. A shift of the centroid of D_{qel} towards a lower energy compared with the centroid of D_{fus} was also observed by Palshetkar *et al.* [30] for the system ${}^6\text{Li} + {}^{197}\text{Au}$. The work in Ref. [30] had also demonstrated that the inclusion of breakup α in defining D_{qel} shifts the centroid of the quasi-elastic barrier distribution to higher energies. This is again consistent with the interpretation of Ref. [14].

In this context, we present our investigation of barrier distributions derived from fusion and quasi-elastic back-scattering measurements for the system ${}^6\text{Li} + {}^{64}\text{Ni}$. We performed the measurement of both fusion and back-angle quasi-elastic excitation functions in a single experiment. The primary motivation for the work is to look for a possible shift in the peaks of the distributions and its interpretation in terms of coupled-channel-model calculations. The paper has been arranged as follows: Section II consists of the description of the experiment. In Sec. III, the extraction of the barrier distribution functions and the subsequent analysis in terms of the coupled channel model calculations have been described. The discussion is presented in Sec. IV, which is followed by the summary and conclusion of the work in Sec. V.

II. EXPERIMENTAL DETAILS

The experiment was carried out at the Pelletron Linac Facility in Mumbai, India. A self-supporting $\sim 99\%$ enriched target of ${}^{64}\text{Ni}$ of thickness $507 \mu\text{g}/\text{cm}^2$, procured from Oak Ridge National Laboratory, USA was used for the present

experiment. The thickness of the target was measured by the α -energy loss method and also verified by using forward-angle Rutherford scattering at low energies. The target, placed at the center of a 21 cm hexagonal chamber, was bombarded with ${}^6\text{Li}$ beam from the pelletron at energies from 11 to 28 MeV. The energy was changed in small steps with the beam current varying from 1 to 4 pA depending on the projectile charge state of 2^+ or 3^+ . The energy loss in the target varies from 400 to 200 keV for this energy range. A monitor detector was placed at 30° with respect to the beam direction. A silicon surface barrier detector of thickness $500 \mu\text{m}$ with an angular opening of $\sim 7.0^\circ$ was positioned at 150° with respect to the beam direction. The back-angle quasi-elastic yield was measured by this detector. No arrangement for particle identification was made. The fusion cross sections were also measured in the same experiment. The characteristic γ rays from the residues were detected with the help of two HPGe detectors placed at 45° and 135° with respect to the beam direction [33]. The detailed experimental setup for the measurement of fusion cross section is discussed in Ref. [34]. The events were recorded using the data acquisition system LAMPS [35]. The number of beam particles was measured with the help of an insulated 1-m-long Faraday cup. The dead time during the acquisition was $\sim 6\%$ to 7% . The dead-time correction was subsequently incorporated in estimating the final yield. The error associated with the data points includes statistical uncertainty as well as the systematic uncertainties from the target thickness measurement and the estimation of the number of beam particles. The uncertainties in the γ -ray yields also include the uncertainty in the efficiency of the detectors. It is to be emphasized that we attempted a simultaneous measurement of fusion and back-angle quasi-elastic cross sections in the present experiment.

In Fig. 1, the energy spectrum from the back-angle particle detector has been shown. The two solid lines mark the region used for determining the quasi-elastic cross section. The observed peaks correspond to the ejectile, ${}^6\text{Li}$, scattered elastically and inelastically from the first excited state of ${}^{64}\text{Ni}$ at 1.345 MeV. Simple kinematic considerations indicate that the region of interest may have contributions from other reaction channels like breakup, $1n$, and $1p$ stripping. These reactions yield α particles having energies that can coincide with the chosen region of interest in the spectrum. The lighter charged fragments from these reactions will have energies lower than the energy region of interest. The long dashed line on the left indicates the energy of the α particle moving with an average velocity equal to the velocity of the ${}^6\text{Li}$ projectile before its elastic breakup while moving in the direction of $150^\circ \pm 3.5^\circ$. The minimum and maximum energy limits of the α particles coming from 2.18 MeV resonant breakup of ${}^6\text{Li}$ moving towards 150° are approximately 4.1 and 9.0 MeV [36]. The energy range of the resonant-breakup α particles is denoted by bu in the figure. Subsequently, we assumed that the region used (represented by the Gaussian peaks) for quasi-elastic yield estimation does not include any significant contribution from breakup of ${}^6\text{Li}$ projectile. However, the contributions from $1n$ -stripping reaction ${}^{64}\text{Ni}({}^6\text{Li}, \alpha p)$ and $1p$ -stripping reaction ${}^{64}\text{Ni}({}^6\text{Li}, \alpha n)$ can be there within the region of interest. The ground state Q values of these reactions are given in Table I.

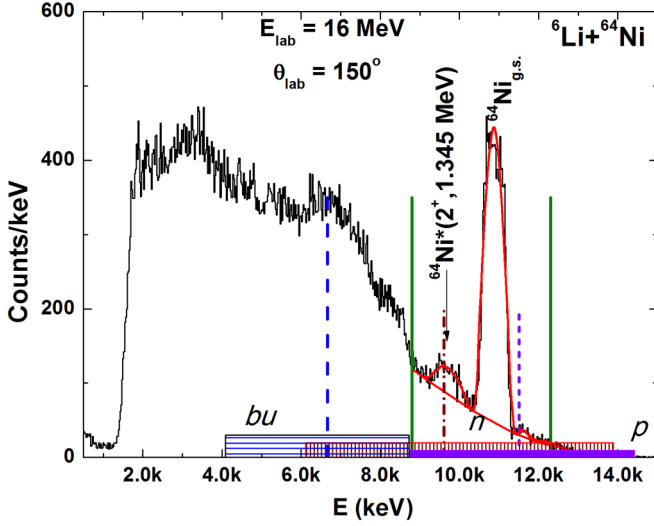


FIG. 1. (Color online) The energy spectrum of the ejectile at $\theta_{\text{lab}} = 150^\circ$ for $E_{\text{lab}} = 16$ MeV. The two solid lines indicate the limits of the region considered for the estimation of quasi-elastic yield. The long dashed line on the left corresponds to the energy of the α particle moving with beam velocity in the direction of $\theta_{\text{lab}} = 150^\circ$ after the breakup of ${}^6\text{Li}$. The dashed-dotted and short dashed lines indicate the energies of α particles moving with the same velocities as the unstable ${}^5\text{Li}$ and ${}^5\text{He}$ ejectiles in the direction of $\theta_{\text{lab}} = 150^\circ$ following the $1n$ - and $1p$ -stripping reactions, respectively. The shaded regions marked by bu , n , and p represent the energy ranges of α particles coming from sequential breakup, $1n$ -, and $1p$ -stripping reactions.

Kinematic estimations suggest that α particles coming from the unstable ${}^5\text{Li}$ and ${}^5\text{He}$ ejectiles will have the energy limits of 6.1 to 13.9 MeV and 8.7 to 14.4 MeV, respectively, in the direction of $\theta_{\text{lab}} = 150^\circ$. The energy ranges of the α particles coming from $1n$ and $1p$ -stripping reactions are shown by shaded regions marked in the figure by n and p , respectively. The vertical dashed-dotted and short dashed lines in the middle of the respective regions denote the average energies of the α particles in the three-body exit channels following the stripping reactions. They will constitute the major part of the continuum below the chosen peaks within the region of interest. In the estimation of the experimental quasi-elastic cross section, only the yields under the selected peaks, as shown in the diagram, have been considered. Therefore, in the subsequent analysis, the quasi-elastic yield (qel) indicates the summed yield of the elastic and the inelastic target excitation processes only.

TABLE I. Q values of different reaction channels.

| Reaction channel | Q_{gg} (MeV) |
|--|----------------|
| ${}^{64}\text{Ni}({}^6\text{Li}, {}^5\text{Li}){}^{65}\text{Ni}$ | 0.435 |
| ${}^{64}\text{Ni}({}^6\text{Li}, {}^7\text{Li}){}^{63}\text{Ni}$ | -2.406 |
| ${}^{64}\text{Ni}({}^6\text{Li}, {}^5\text{He}){}^{65}\text{Cu}$ | 3.021 |
| ${}^{64}\text{Ni}({}^6\text{Li}, {}^4\text{He}){}^{66}\text{Cu}$ | 10.822 |
| ${}^{64}\text{Ni}({}^6\text{Li}, {}^2\text{H}){}^{68}\text{Zn}$ | 3.859 |

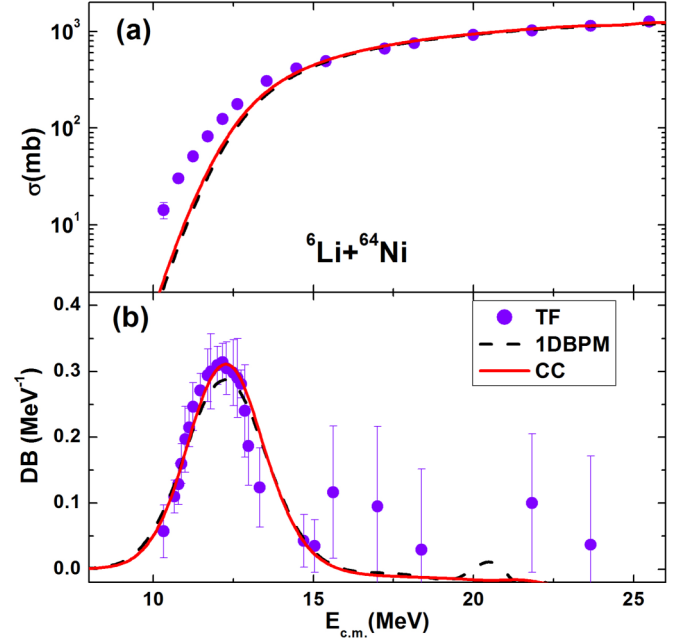


FIG. 2. (Color online) (a) The experimental fusion excitation function has been shown in comparison with the one dimensional barrier penetration model (1DBPM) and CC model predictions. (b) Corresponding barrier distribution functions (DB). The energy values include the target thickness correction and the uncertainty restricted within the width of the symbol.

III. ANALYSIS AND RESULTS

A. Fusion excitation functions and barrier distribution

The fusion excitation function of ${}^6\text{Li} + {}^{64}\text{Ni}$, shown in Fig. 2(a), has already been reported in Ref. [34]. The data points in the diagram represent the total fusion (TF) cross sections, the sum of the cross sections for the processes of complete fusion (CF), and incomplete fusion (ICF) of one of the fragments following the breakup of ${}^6\text{Li}$ into α and d clusters at each incident energy. The experimental cross sections were determined from the cross sections of the residues produced in $2n$, $3n$, and pn channels from pure CF decay and $p2n/dn$, αn , and $\alpha 2n$ channels from CF as well as ICF processes. The d -ICF channel, (${}^6\text{Li}$, αn), can also have contribution from deuteron transfer or d transfer ($Q = 10.822$ MeV; Table I) to unbound states of the residue followed by $1n$ decay and from the $1p$ -stripping channel ($Q = 3.021$ MeV) leading to three-body final states. These processes are experimentally indistinguishable. Hence the TF cross sections plotted include CF, α -ICF, d -ICF and/or d -stripping and p -stripping cross sections. The dashed curve in the figure represents the one-dimensional barrier penetration model (1DBPM) prediction using the Akyüz–Winther potential [37] with parameters $V_0 = 41.47$ MeV, $r_0 = 1.17$ fm, and $a_0 = 0.60$ fm in the code CCFULL [38] in the no-coupling mode. The code CCFULL yields the CF cross section in the absence of any ICF process. In the above barrier region, with negligible effect of channel coupling, the 1DBPM cross sections reproduced the measured TF (=CF + ICF) cross sections quite well. The resultant barrier height V_B , barrier radius R_B , and barrier width $\hbar\omega$ obtained

from the calculation are 12.41 MeV, 9.1 fm, and 3.9 MeV, respectively. In the top of and below the barrier region, 1DBPM prediction largely underpredicts the data. A CC calculation was subsequently performed with the code CCFULL including the coupling to the first-excited state 2^+ (1.345 MeV) of ^{64}Ni and the first resonant state 3^+ (2.18 MeV) of the projectile ^6Li . No significant improvement is observed in the reproduction of the lower-energy fusion excitation function although there is slight enhancement in the cross section values (solid curve).

If $\sigma_{\text{fus}}(E_{\text{c.m.}})$ were the fusion cross section for a system at the projectile energy $E_{\text{c.m.}}$ in the center-of-mass system, then the fusion barrier distribution $D_{\text{fus}}(E_{\text{c.m.}})$ is defined as

$$D_{\text{fus}}(E_{\text{c.m.}}) = \frac{1}{\pi R_B^2} \frac{d^2(E_{\text{c.m.}}\sigma_{\text{fus}})}{dE_{\text{c.m.}}^2}, \quad (1)$$

where R_B is the uncoupled barrier radius [1].

The barrier distribution was obtained from the fusion excitation function by the point difference method using the above relation. The experimental D_{fus} is shown in the lower panel of Fig. 2 while the theoretical D_{fus} from 1DBPM and CC calculations are shown by dashed and solid lines, respectively. Very good agreement between the derived data and the coupled-channel prediction is observed for the barrier distribution function. The expression of channel coupling is more prominent in barrier distribution function compared to the fusion excitation function. Two things to be noted here: First, the experimental and theoretical barrier distribution functions peak at the center-of-mass energy value close to the Coulomb barrier of the system ($V_{\text{C.B.}} \simeq 12.8$ MeV). This indicates that, for fusion reaction of weakly bound projectile ^6Li with ^{64}Ni target, the Coulomb barrier is the reaction threshold. Coupling to the inelastic excitations of the target or projectile does not shift the peak position of the distribution. Second, the enhancement in the peak strength of the distribution function, achieved with the inelastic coupling over the uncoupled 1DBPM calculation, implies attachment of more *weight* to the nominal Coulomb barrier for fusion reaction.

B. Quasi-elastic excitation function and barrier distribution

The quasi-elastic excitation function has been obtained from the silicon surface barrier detector placed at 150° with respect to beam direction. The cross section was estimated by using the working formula

$$\sigma(E) = \frac{Y}{N_B N_T \Omega}, \quad (2)$$

where Y is the total yield under the peaks in the region of interest, N_B is the number of beam particles, and N_T is the number of target particles per unit area. Ω is the solid angle subtended by the detector at the target position.

The barrier distribution, D_{qel} , was derived from the back-angle data [2] by using the point difference formula

$$D_{\text{qel}}(E) = -\frac{d}{dE} \left(\frac{d\sigma_{\text{qel}}}{d\sigma_R} \right), \quad (3)$$

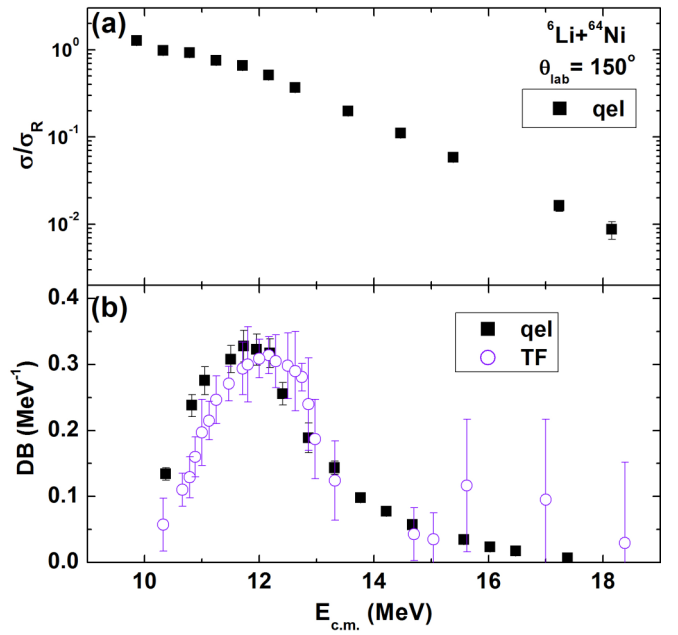


FIG. 3. (Color online) Back angle ($\theta_{\text{lab}} = 150^\circ$) quasi-elastic excitation function plotted in upper panel. The quasi-elastic cross section was estimated using the yields under the peaks marked in Fig. 1. The yields under consideration predominantly comes from the elastic scattering and inelastic scattering from the 1.345 MeV first-excited state of ^{64}Ni . In the lower panel, the derived data of quasi-elastic barrier distribution has been shown by solid squares. For comparison, the fusion-barrier distribution obtained from the TF excitation function has been shown by open circles. DB denotes barrier distribution function in the lower panel. The energy values corresponding to fusion barrier distribution includes the correction due to the target thickness while that corresponding to the quasi-elastic distribution includes target thickness as well as centrifugal correction of Eq. 4.

where $d\sigma_{\text{qel}}$ and $d\sigma_R$ are the differential cross sections for the quasi-elastic and the Rutherford scattering, respectively, at $\theta_{\text{lab}} = 150^\circ$. Following the conservation of flux argument, D_{qel} from the quasi-elastic cross section at 180° and D_{fus} are equal to each other [39]. Since the measurement was done at less than 180° , a *centrifugal correction* is needed to estimate the effective energy. If the detector were placed at the center-of-mass angle of $\theta_{\text{c.m.}}$ for the center-of-mass energy $E_{\text{c.m.}}$, then the effective energy after the centrifugal correction [2] is

$$E_{\text{eff}} = E_{\text{c.m.}} \frac{2}{\text{cosec}(\theta_{\text{c.m.}}/2) + 1}. \quad (4)$$

The ratio of the quasi-elastic scattering cross section to the Rutherford cross section at 150° for the $^6\text{Li} + ^{64}\text{Ni}$ system is plotted in the upper panel of Fig. 3. In the lower panel, the derived data of quasi-elastic barrier distribution, D_{qel} , (solid squares) as a function of effective incident energy (after correcting for the target thickness) is shown. The fusion-barrier distribution function, D_{fus} , has also been overlaid on D_{qel} for comparison. One can observe from Fig. 3(b) that the location of the peak in D_{qel} is shifted distinctly towards a lower incident

energy in comparison to the peak position of D_{fus} . As has been pointed out by Zagrebaev [14], the shift of the D_{qel} peak towards a lower incident energy indicates that the Coulomb barrier is no longer the reaction threshold for the quasi-elastic processes. We performed a detailed coupled reaction channel (CRC) calculation to look into this aspect.

C. Coupled reaction channel calculation

The coupled reaction channel (CRC) calculation to obtain the quasi-elastic excitation function for ${}^6\text{Li} + {}^{64}\text{Ni}$ was carried out by using the code FRESKO (version FRES 2.9) [40].

In the first step, the CRC calculation was performed by coupling only the low-lying inelastic excitations, the first-excited state (2^+ , 1.345 MeV) of the target ${}^{64}\text{Ni}$, and the resonant first-excited state (3^+ , 2.18 MeV) of the ${}^6\text{Li}$ projectile (CC I).

The diagonal potential used in the entrance channel is composed of the Coulomb potential plus the *bare* nuclear potential with real and imaginary components. A point charge interacting with a uniform charged sphere of radius $R_C = r_c(A_P^{1/3} + A_T^{1/3})$, where A_P and A_T are the mass numbers of the projectile and target, respectively, and with $r_c = 1.3$ fm was assumed for deriving the Coulomb potential. The real part of the *bare* nuclear potential was taken to be of double-folding (DF) model potential [41] with normalization $N_r = 1.0$. The DF potential was generated using the M3Y-Reid nucleon-nucleon interaction with an energy-independent zero-range exchange potential. The density dependence of the interaction (DDM3Y) was taken from Ref. [42]. The point nucleon density for ${}^{64}\text{Ni}$, to generate the DF potential, was obtained from Ref. [43]. A parametric form for the charge distribution of ${}^6\text{Li}$ was taken from Ref. [41], which was unfolded to obtain the point proton distribution. Assuming the neutron distribution to have the same shape as the proton distribution for $N = Z$ ${}^6\text{Li}$ nucleus, the matter density of ${}^6\text{Li}$ was derived. The details of the generation of the DF potential for ${}^6\text{Li} + {}^{64}\text{Ni}$ system is given in Ref. [44]. The imaginary part of the *bare* potential of Woods–Saxon shape was assumed to have a very short range to simulate the ingoing-wave boundary condition [45] for the core fusion process. The chosen values of the strength W_0 , radius r_0 , and diffuseness a_0 are displayed in Table II.

TABLE II. Potential parameters used in CRC calculation.

| Channel | V_0 (MeV) | r_0 (fm) | a_0 (fm) | W_0 (MeV) | r_w (fm) | a_w (fm) |
|------------------------------------|----------------|---------------|---------------|----------------|---------------|---------------|
| ${}^6\text{Li} + {}^{64}\text{Ni}$ | (Folded) | Pot. with | $N_r = 1.0$ | 50.0 | 1.0 | 0.25 |
| ${}^5\text{Li} + {}^{65}\text{Ni}$ | 41.22 | 1.17 | 0.593 | 50.0 | 1.0 | 0.25 |
| ${}^5\text{He} + {}^{65}\text{Cu}$ | 37.75 | 1.17 | 0.593 | 50.0 | 1.0 | 0.25 |
| $n + {}^5\text{Li}$ | $V_{b.s.}^a$ | 1.25 | 0.65 | | | |
| $n + {}^{64}\text{Ni}$ | $V_{b.s.}$ | 1.25 | 0.65 | | | |
| $p + {}^5\text{He}$ | $V_{b.s.}$ | 1.25 | 0.65 | | | |
| $p + {}^{64}\text{Ni}$ | $V_{b.s.}$ | 1.25 | 0.65 | | | |
| ${}^5\text{Li} + {}^{64}\text{Ni}$ | 40.95 | 1.17 | 0.593 | | | |
| ${}^5\text{He} + {}^{64}\text{Ni}$ | 37.42 | 1.17 | 0.593 | | | |

^aSearched to reproduce the binding energy.

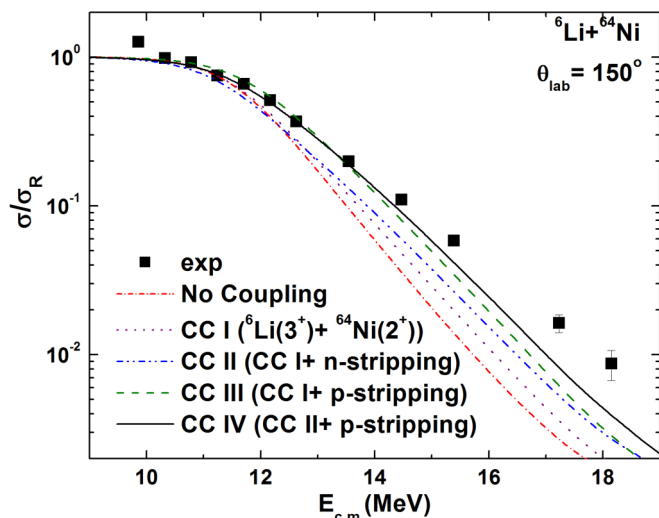


FIG. 4. (Color online) The quasi-elastic excitation functions from CRC calculation with different coupling conditions in comparison with the data (■). The *dashed-dotted* curve represents the excitation function in no coupling condition. The CC I (dotted) curve stands for inelastic coupling only while CC II (dashed-double dotted) stands for the condition CC I + $1n$ stripping. The CC III (dashed curve) condition denotes the coupling scheme of CC I + $1p$ stripping and CC IV (solid curve) is for the coupling scheme that includes inelastic, $1n$ - and $1p$ -stripping channels.

The nondiagonal or transition potentials for inelastic channels were obtained by deforming the entrance channel potential with the coupling strengths determined from the respective reduced transition probabilities. The reduced transition probability $B(E2)$ for the $E2$ transition from 0^+ to 2^+ (1.345 MeV) excited state of the target ${}^{64}\text{Ni}$ was taken to be $760 e^2 \text{fm}^4$ [46]. A reduced transition probability, $B(E2) = 25.6 e^2 \text{fm}^4$ for the 1^+ ground state to the 3^+ (2.18 MeV) resonant state transition in ${}^6\text{Li}$ projectile was taken from Ref. [29]. The Coulomb matrices and the nuclear deformation lengths for the coupled channel calculations were estimated from the $B(E2)$ values. Reorientation terms were also considered in the coupling scheme. The excited-state quadrupole moment of the 3^+ excited state of ${}^6\text{Li}$ was obtained from Ref. [29]. The diagonal coupling matrix element for the excited-state reorientation term for ${}^{64}\text{Ni}$ was estimated from the reduced transition probability by assuming a rotational model. The resultant excitation function and barrier distribution (dotted curves) from the CC I coupling scheme are compared with the data and with the outputs of the no-coupling condition (dash-dotted curve) in Figs. 4 and 5.

In the coupled-channel scheme CC II, along with the inelastic channels, the one-neutron-stripping channel ($Q_{gg} = 0.435$ MeV) was also included in the coupling scheme. The low-lying negative parity states of the residual nucleus ${}^{65}\text{Ni}$ included in the scheme are given in Table III. The spectroscopic amplitudes (SA) of $\langle {}^5\text{Li} | {}^6\text{Li} \rangle$ and $\langle {}^{65}\text{Ni} | {}^{64}\text{Ni} \rangle$ overlaps are also shown in Table III and are taken from Refs. [47,48]. Akyüz–Winther potential was used for the outgoing transfer channel. The relevant parameters are shown in Table II. The strengths of the bound-state potential parameters were adjusted

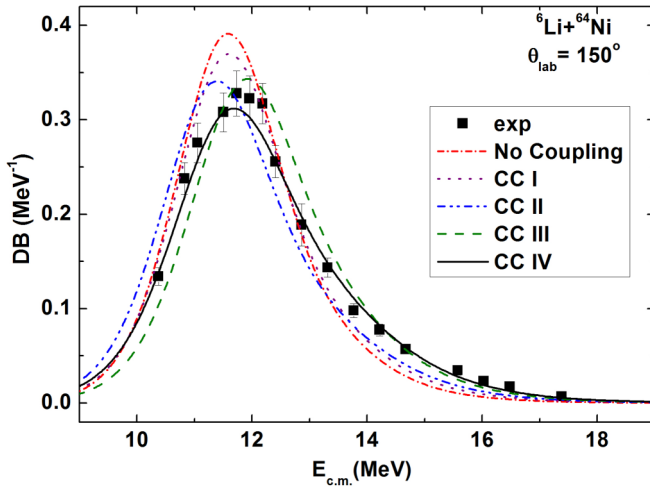


FIG. 5. (Color online) The barrier distribution extracted from the calculated quasi-elastic excitation functions in comparison derived barrier distribution data (■). For the description of the curves, see Fig. 4.

to reproduce the neutron binding energies for the states of ^{65}Ni nucleus with the radius parameter $r_0 = 1.25$ fm and diffuseness $a_0 = 0.65$ fm. The parameters used for $^5\text{Li} + ^{64}\text{Ni}$ core-core potential were also derived by assuming the Akyüz–Winther potential and are shown in Table II. The calculated quasi-elastic excitation function and the corresponding barrier distribution are displayed in Figs. 4 and 5 by the dash-double dotted lines.

To further investigate the effect of transfer coupling on quasi-elastic excitation function and barrier distribution, in the scheme CC III we coupled the one-proton-stripping channel with $Q_{gg} = 3.021$ MeV switching off the one-neutron transfer channel. Five low-lying negative-parity states of ^{65}Cu were coupled along with the inelastic channels included in the scheme CC I. The spectroscopic amplitudes associated with the $\langle ^{65}\text{Cu} | ^{64}\text{Ni} \rangle$ overlaps are taken from Ref. [49]. As in the case of CC II, the Akyüz–Winther potential form with parameters listed in Table II had been used in the exit channel. The radius and the diffuseness parameters for the bound-state

TABLE III. Spectroscopic amplitudes of the overlaps used in the CRC calculation.

| Nucleus | E^* (MeV) | J^π | Core | nlj | SA | Ref. |
|------------------|-------------|---------|---------------------------|------------|--------|------|
| ^6Li | | | $^5\text{Li}/^5\text{He}$ | $1p_{3/2}$ | 0.5640 | [47] |
| ^6Li | 0.000 | 1^+ | $^5\text{Li}/^5\text{He}$ | $1p_{1/2}$ | 0.5804 | [47] |
| ^{65}Ni | 0.000 | $5/2^-$ | ^{64}Ni | $1f_{5/2}$ | 0.4669 | [48] |
| ^{65}Ni | 0.063 | $1/2^-$ | ^{64}Ni | $2p_{1/2}$ | 0.6317 | [48] |
| ^{65}Ni | 0.310 | $3/2^-$ | ^{64}Ni | $2p_{3/2}$ | 0.1483 | [48] |
| ^{65}Ni | 0.693 | $3/2^-$ | ^{64}Ni | $2p_{3/2}$ | 0.3050 | [48] |
| ^{65}Cu | 0.000 | $3/2^-$ | ^{64}Ni | $2p_{3/2}$ | 0.8889 | [49] |
| ^{65}Cu | 0.771 | $1/2^-$ | ^{64}Ni | $2p_{1/2}$ | 0.8660 | [49] |
| ^{65}Cu | 1.116 | $5/2^-$ | ^{64}Ni | $1f_{5/2}$ | 0.5099 | [49] |
| ^{65}Cu | 1.482 | $7/2^-$ | ^{64}Ni | $1f_{7/2}$ | 0.2236 | [49] |
| ^{65}Cu | 1.622 | $5/2^-$ | ^{64}Ni | $1f_{5/2}$ | 0.7550 | [49] |

potential were chosen to be 1.25 and 0.65 fm, respectively. The strengths were adjusted to reproduce the proton binding energies in the states considered for ^{65}Cu . The parameters of the potential used are given in Table II. The dashed lines in Figs. 4 and 5 represent the results from CC III scheme.

Finally, in the coupling scheme denoted by CC IV both the one-neutron- and the one-proton-stripping channels, as described above, were coupled in addition to the inelastic channels of CC I. The solid lines in the Figs. 4 and 5 depict the resultant quasi-elastic excitation function and the barrier distribution.

IV. DISCUSSION

Two major observations come out from the analyses. First, the barrier distribution, D_{fus} , extracted from the measured TF excitation function for the $^6\text{Li} + ^{64}\text{Ni}$ system, is quite well reproduced, in magnitude and shape, with the introduction of inelastic coupling to the first-excited states of ^6Li and ^{64}Ni in the barrier-penetration model. The model, however, underpredicts the excitation-function data in the below-barrier region (Fig. 2), improving marginally over the 1DBPM prediction. The magnitude of the model barrier distribution function at the peak position in the CC condition is enhanced compared to the 1DBPM result. The location of the peak is very close to the Coulomb-barrier energy of the system. Second, the barrier distribution, D_{qel} , extracted from back-angle quasi-elastic excitation function is found to be shifted to lower energy by about 450 keV compared to D_{fus} [Fig. 3(b)]. The observation corroborates the inferences drawn by Zagrebaev [14] and Monteiro *et al.* [22,31] for heavier targets that, for weakly bound projectiles, the reaction barrier does not coincide with the Coulomb barrier. The reaction threshold in such cases is shifted towards a lower incident energy although the shift is smaller in case of lower-mass targets.

Subsequently, detailed coupled reaction channel (CRC) calculations were performed to describe the back-angle quasi-elastic excitation function and the derived barrier distribution function (Figs. 4 and 5). The coupling to the first-excited state (2^+ , 1.345 MeV) of ^{64}Ni and the resonant first-excited state (3^+ , 2.18 MeV) of ^6Li enhances the cross sections at higher energies compared to the no-coupling condition and lowers the peak strength of the barrier distribution. But the overall reproductions of excitation function and D_{qel} are not satisfactory. Also, note that the peaks from the calculations are located at a lower energy with respect to the derived data.

With the introduction of the positive Q -value $1n$ stripping to the low-lying excited states of the residue ^{65}Ni in the coupling scheme (CC II), the excitation function is further enhanced at higher energies. But it is somewhat suppressed at energies below $E_{\text{c.m.}} \sim 12$ MeV. The barrier distribution is shifted considerably towards lower energy, although the magnitude has come down significantly. It appears that the coupling to the positive Q -value neutron-stripping channel shifts the location of the effective reaction barrier to lower energies. The trend, however, does not correspond to the derived barrier distribution data. If instead of $1n$ stripping, the positive Q -value one-proton stripping to low-lying negative-parity states

of the recoiling ${}^{65}\text{Cu}$ are coupled (CC III), the resultant excitation function reproduces the data fairly well in the energy region below 13 MeV. But the model excitation function still falls short at energies above 13 MeV. The calculated distribution function now shifts towards higher energy and the high-energy tail part describes the data points beyond 14 MeV reasonably well. On the other hand, if both $1n$ - and $1p$ -stripping channels are included simultaneously (CC IV), the description of the high-energy part of the excitation function improves further with a good reproduction of the data below 14 MeV. However, excellent reproduction of the quasi-elastic barrier distribution data is observed for the low-energy rising part and the high-energy falling part with the CC IV coupling scheme. Only the peak strength of the model distribution function appears to be slightly lower than the experimental distribution. Interestingly, the peak of the model quasi-elastic barrier distribution function with the CC IV coupling scheme that best describes the data is shifted towards lower energy by about 550 keV compared with the peak position of the fusion-barrier distribution predicted by the CC calculation. The result corroborates with the observed shift in the peak positions of the experimental quasi-elastic and fusion-barrier distributions.

Effect of coupling to $\frac{9}{2}^+$ state

To investigate further the effect of coupling in reproducing the quasi-elastic excitation function, especially the high-energy part, and the corresponding effect on the barrier distribution function, we extended the CRC calculation by including the positive-parity $\frac{9}{2}^+$ states of the residues ${}^{65}\text{Cu}$ ($E^* = 2.54$ MeV) and ${}^{65}\text{Ni}$ ($E^* = 1.017$ MeV). The results of the CRC calculations are shown in Fig. 6. The residues are populated due to the stripped particle occupying the $1g_{\frac{7}{2}}$ single-particle states with transfer angular momentum being $4\hbar$. According to Refs. [48,49], the states have large spectroscopic amplitudes of 0.5385 (for ${}^{64}\text{Ni} + p$) and 0.8591 (for ${}^{64}\text{Ni} + n$). If $1p$ stripping to ${}^{65}\text{Cu}(\frac{9}{2}^+)$ is included in the scheme of CC IV, then excellent reproduction of back-angle quasi-elastic excitation is achieved until $E_{c.m.} \sim 15$ MeV. But the description of the barrier distribution becomes slightly worse with the magnitude of the peak being reduced. If the $1n$ -stripping channel populating the ${}^{65}\text{Ni}(\frac{9}{2}^+)$ residue is coupled as well, the model calculation slightly overpredicts that data at the higher-energy region beyond 15 MeV. But the excitation function in the lower-energy range produces equivalent description of the data like that obtained with the CC IV scheme. Consequently, the calculated barrier distribution reproduces the low-energy barrier distribution data up to the peak quite nicely. On the higher energy-side the model prediction is slightly depressed compared to the data around the 14 MeV energy.

V. SUMMARY AND CONCLUSION

A measurement of total fusion for the system ${}^6\text{Li} + {}^{64}\text{Ni}$ was performed in the incident-energy range of 11 to 28 MeV. Simultaneous measurement of the back-angle quasi-elastic

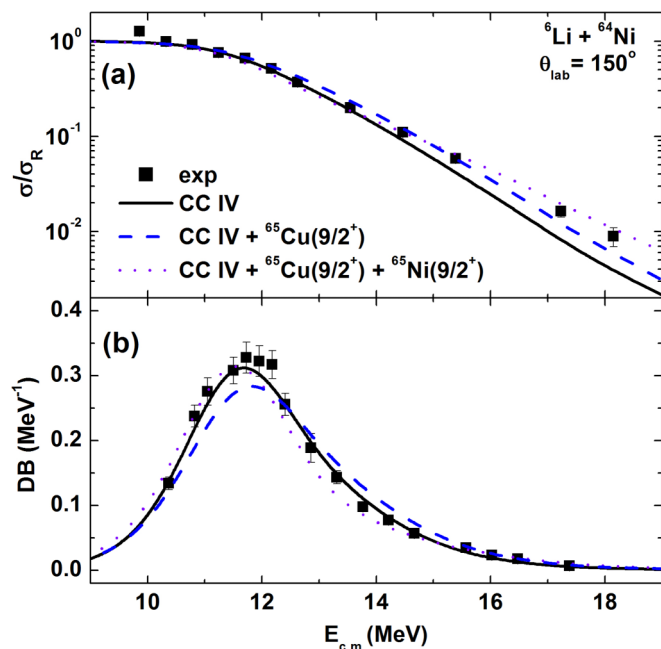


FIG. 6. (Color online) The experimental quasi-elastic excitation function (upper panel) and corresponding barrier distribution function (denoted by DB in the lower panel) compared with the CRC calculation that includes the coupling to positive parity $\frac{9}{2}^+$ states in residues ${}^{65}\text{Cu}$ and ${}^{65}\text{Ni}$ from the reactions (${}^6\text{Li}$, ${}^5\text{He}$) and (${}^6\text{Li}$, ${}^5\text{Li}$) along with the coupling scheme CC IV (see text).

excitation functions in the energy range of 11 to 20 MeV was also carried out. Barrier distributions from the respective excitation functions were extracted. The quasi-elastic barrier distribution function was primarily constructed out of the elastic and the target inelastic excitation contributions. The data indicate that the peak of the quasi-elastic barrier distribution is located at an energy that is about 450 keV lower than the peak position of the fusion-barrier distribution. A similar shift in the peak positions of the two distribution functions was reported earlier for heavier targets. The shifts were larger in those cases. It was conjectured that the quasi-elastic barrier distribution actually represents the reaction threshold distribution and is not identical to the fusion-barrier distribution. However, a systematic investigation of the magnitude of shift in the peaks of the barrier distributions as a function of target mass for a particular projectile appears to be very interesting and worth investigating. Further measurements for this purpose over different target mass region are also required.

Detailed coupled-channel calculations were performed to describe the excitation functions as well as the barrier distributions in order to see the effect of coupling on the observables. The coupling to the low-lying inelastic excitations of the ${}^{64}\text{Ni}$ target and the to the resonant first excited state of ${}^6\text{Li}$ projectile could describe the fusion-barrier distribution to a good extent but underpredicts the excitation function data at lower energies. Inclusion of the coupling to the transfer channels to describe the low-energy behavior of the excitation function and the barrier distribution is important and the effect needs to be explored. On the other hand, the single-particle transfer

channels leading to three-body final states appear to play important roles in the reproduction of quasi-elastic barrier distribution. Inclusion of one-proton ($Q_{gg} = 3.021$ MeV) and one-neutron ($Q_{gn} = 0.435$ MeV) stripping channels in the coupling scheme of the inelastic excitations of ${}^6\text{Li}$ and ${}^{64}\text{Ni}$ in the CRC model calculation produces an excellent agreement with the barrier distribution, although the excitation function at higher energies remains underpredicted. Subsequent introduction of coupling to $\frac{9}{2}^+$ states of ${}^{65}\text{Cu}$ and ${}^{65}\text{Ni}$ residues improves the reproduction of the quasi-elastic excitation function further and also well describes the quasi-elastic barrier distribution data.

In conclusion, we would like to mention that a definite shift in the peaks of the barrier distributions is observed for the weakly bound ${}^6\text{Li}$ projectile reaction with a medium-mass ${}^{64}\text{Ni}$ target. The observation is also supported by the subsequent coupled-channel calculations. Also, the coupling to one-nucleon stripping channels with positive Q values leading to three body final states is found to describe the quasi-

elastic barrier distribution and excitation functions quite nicely. To clearly identify the reaction mechanisms contributing in generating the shape and the magnitude of the quasi-elastic barrier distribution, more precise experiment with proper channel selections is absolutely necessary.

ACKNOWLEDGMENTS

The authors would like to thank the technical staff of the Pelletro and Professor R. Palit of DNAP, TIFR and Dr. R. Tripathy, RCD, BARC for their support and cooperation during the experiment. The authors gratefully acknowledge Professor N. Keeley and Professor A. Moro for their fruitful suggestions and help in carrying out the CRC calculation. The authors also acknowledge Professor H. Majumdar for patiently going through the manuscript and his suggestions for improvement. Md. Moin Shaikh and S. Rajbanshi thank the Council of Scientific & Industrial Research, Govt. of India, for the financial support.

-
- [1] N. Rowley, G. R. Satchler and P. H. Stelson, *Phys. Lett. B* **254**, 25 (1991).
- [2] H. Timmers, J. R. Leigh, M. Dasgupta, D. J. Hinde, R. C. Lemmon, J. C. Mein, C. R. Morton, J. O. Newton, and N. Rowley, *Nucl. Phys. A* **584**, 190 (1995).
- [3] M. Dasgupta, D. J. Hinde, N. Rowley, and A. M. Stefanini, *Annu. Rev. Nucl. Part. Sci.* **48**, 401 (1998).
- [4] S. G. Steadman and M. J. Rhoades-Brown, *Annu. Rev. Nucl. Part. Sci.* **36**, 649 (1986).
- [5] M. Beckerman, *Rep. Prog. Phys.* **51**, 1047 (1988).
- [6] C. H. Dasso, S. Landowne, and A. Winther, *Nucl. Phys. A* **405**, 381 (1983); **407**, 221 (1983).
- [7] R. A. Broglia, C. H. Dasso, S. Landowne, and A. Winther, *Phys. Rev. C* **27**, 2433(R) (1983).
- [8] G. R. Satchler, *Phys. Rep.* **199**, 147 (1991).
- [9] B. B. Back, H. Esbensen, C. L. Jiang, and K. E. Rehm, *Rev. Mod. Phys.* **86**, 317 (2014).
- [10] K. Hagino and N. Takigawa, *Prog. Theor. Phys.* **128**, 1001 (2012).
- [11] L. F. Canto, P. R. S. Gomes, R. Donangelo, and M. S. Hussein, *Phys. Rep.* **424**, 1 (2006).
- [12] K. Hagino and N. Rowley, *Phys. Rev. C* **69**, 054610 (2004).
- [13] H. Timmers, D. Ackermann, S. Beghini, L. Corradi, J. H. He, G. Montagnoli, F. Scarlassara, A. M. Stefanini, and N. Rowley, *Nucl. Phys. A* **633**, 421 (1998).
- [14] V. I. Zagrebaev, *Phys. Rev. C* **78**, 047602 (2008).
- [15] S. Mitsuoka, H. Ikezoe, K. Nishio, K. Tsuruta, S. C. Jeong, and Y. Watanabe, *Phys. Rev. Lett.* **99**, 182701 (2007).
- [16] S. S. Ntshangase, N. Rowley, R. A. Bark, S. V. Förtsch, J. J. Lawrie, E. A. Lawrie, R. Lindsay, M. Lipoglavsek, S. M. Maliage, L. J. Mudau, S. M. Mullins, O. M. Ndwandwe, R. Neveling, G. Sletten, F. D. Smit, and C. Theron, *Phys. Lett. B* **651**, 27 (2007).
- [17] M. Dasgupta, P. R. S. Gomes, D. J. Hinde, S. B. Moraes, R. M. Anjos, A. C. Berriman, R. D. Butt, N. Carlin, J. Lubian, C. R. Morton, J. O. Newton and A. Szanto de Toledo, *Phys. Rev. C* **70**, 024606 (2004).
- [18] M. Dasgupta, D. J. Hinde, R. D. Butt, R. M. Anjos, A. C. Berriman, N. Carlin, P. R. S. Gomes, C. R. Morton, J. O. Newton, A. Szanto de Toledo, and K. Hagino, *Phys. Rev. Lett.* **82**, 1395 (1999).
- [19] C. Signorini, Z. H. Liu, Z. C. Li, K. E. G. Löbner, L. Müller, M. Ruan, K. Rudolph, F. Soramel, C. Zotti, A. Andrighetto, L. Stroe, A. Vitturi, and H. Q. Zhang, *Eur. Phys. J. A* **5**, 7 (1999).
- [20] M. Dasgupta, D. J. Hinde, K. Hagino, S. B. Moraes, P. R. S. Gomes, R. M. Anjos, R. D. Butt, A. C. Berriman, N. Carlin, C. R. Morton, J. O. Newton and A. Szanto de Toledo, *Phys. Rev. C* **66**, 041602(R) (2002).
- [21] C. J. Lin, H. Q. Zhang, F. Yang, M. Ruan, Z. H. Liu, Y. W. Wu, X. K. Wu, P. Zhou, C. L. Zhang, G. L. Zhang, G. P. An, H. M. Jia, and X. X. Xu, *Nucl. Phys. A* **787**, 281 (2007).
- [22] D. S. Monteiro, O. A. Capurro, A. Arazi, J. O. Fernández Niello, J. M. Figueira, G. V. Martí, D. Martínez Heimann, A. E. Negri, A. J. Pacheco, V. Guimarães, D. R. Otomar, J. Lubian, and P. R. S. Gomes, *Phys. Rev. C* **79**, 014601 (2009).
- [23] S. Mukherjee, B. K. Nayak, D. S. Monteiro, J. Lubian, P. R. S. Gomes, S. Appannababu, and R. K. Choudhury, *Phys. Rev. C* **80**, 014607 (2009).
- [24] D. R. Otomar, J. Lubian, P. R. S. Gomes, D. S. Monteiro, O. A. Capurro, A. Arazi, J. O. Fernández Niello, J. M. Figueira, G. V. Martí, D. Martínez Heimann, A. E. Negri, A. J. Pacheco, V. Guimarães, and L. C. Chamon, *Phys. Rev. C* **80**, 034614 (2009).
- [25] K. Zerva, N. Patronis, A. Pakou, N. Alamanos, X. Aslanoglou, D. Filipescu, T. Glodariu, M. Kokkoris, M. La Commara, A. Lagoyannis, M. Mazzocco, N. G. Nicolis, D. Pierroutsakou, M. Romoli, and K. Rusek, *Phys. Rev. C* **80**, 017601 (2009).
- [26] K. Zerva, A. Pakou, K. Rusek, N. Patronis, N. Alamanos, X. Aslanoglou, D. Filipescu, T. Glodariu, N. Keeley, M. Kokkoris, M. La Commara, A. Lagoyannis, M. Mazzocco, N. G. Nicolis, D. Pierroutsakou, and M. Romoli, *Phys. Rev. C* **82**, 044607 (2010).

- [27] K. Zerva, A. Pakou, N. Patronis, P. Figuera, A. Musumarra, A. Di Pietro, M. Fisichella, T. Glodariu, M. La Commara, M. Lattuada, M. Mazzocco, M. G. Pellegriti, D. Pierroutsakou, A. M. Sanchez-Benitez, V. Scuderi, E. Strano, and K. Rusek, *Eur. Phys. J. A* **48**, 102 (2012).
- [28] H. M. Jia, C. J. Lin, H. Q. Zhang, Z. H. Liu, N. Yu, F. Yang, F. Jia, X. X. Xu, Z. D. Wu, S. T. Zhang, and C. L. Bai, *Phys. Rev. C* **82**, 027602 (2010).
- [29] M. Zadro, P. Figuera, A. Di Pietro, M. Fisichella, M. Lattuada, T. Lönnroth, M. Milin, V. Ostashko, M. G. Pellegriti, V. Scuderi, D. Stanko, E. Strano, and D. Torresi, *Phys. Rev. C* **87**, 054606 (2013).
- [30] C. S. Palshetkar, Shital Thakur, V. Nanal, A. Shrivastava, N. Dokania, V. Singh, V. V. Parkar, P. C. Rout, R. Palit, R. G. Pillay, S. Bhattacharyya, A. Chatterjee, S. Santra, K. Ramachandran, and N. L. Singh, *Phys. Rev. C* **89**, 024607 (2014).
- [31] D. S. Monteiro, P. R. S. Gomes, and J. Lubian, *Phys. Rev. C* **80**, 047602 (2009).
- [32] P. K. Rath, S. Santra, N. L. Singh, R. Tripathi, V. V. Parkar, B. K. Nayak, K. Mahata, R. Palit, Suresh Kumar, S. Mukherjee, S. Appannababu, and R. K. Choudhury, *Phys. Rev. C* **79**, 051601(R) (2009).
- [33] P. R. S. Gomes, T. J. P. Penna, R. Liguori Neto, J. C. Acquadro, C. Teneiro, P. A. B. Freitas, E. Crema, N. Carlin Filho, and M. M. Coimbra, *Nucl. Instrum. Methods Phys. Res., Sect. A* **280**, 395 (1989).
- [34] Md. Moin Shaikh, Subinit Roy, S. Rajbanshi, M. K. Pradhan, A. Mukherjee, P. Basu, S. Pal, V. Nanal, R. G. Pillay, and A. Shrivastava, *Phys. Rev. C* **90**, 024615 (2014).
- [35] Computer code LAMPS (Linux Advanced Multiparameter System), www.tifr.res.in/~pl2X-sim-pell/lamps.html
- [36] K. O. Pfeiffer, E. Speth, and K. Bethge, *Nucl. Phys. A* **206**, 545 (1973).
- [37] O. Akyüz and A. Winther, *Proc. Int. School of Physics Enrico Fermi, Course LXXVII*, edited by R. A. Broglia, R. A. Ricci, and C. H. Dasso (Noah-Holland, Amsterdam, 1981), p. 492.
- [38] K. Hagino, N. Rowley, and A. T. Kruppa, *Comput. Phys. Commun.* **123**, 143 (1999).
- [39] A. B. Balantekin and P. E. Reimer, *Phys. Rev. C* **33**, 379 (1986).
- [40] I. J. Thompson, *Comput. Phys. Rep.* **7**, 167 (1988).
- [41] G. R. Satchler and W. G. Love, *Phys. Rep.* **55**, 183 (1979).
- [42] Dao T. Khoa and W. von Oertzen, *Phys. Lett. B* **304**, 8 (1993); Dao T. Khoa, W. von Oertzen, and H. G. Bohlen, *Phys. Rev. C* **49**, 1652 (1994).
- [43] <http://www-nds.iaea.org/RIPL-2>
- [44] M. Biswas, Subinit Roy, M. Sinha, M. K. Pradhan, A. Mukherjee, P. Basu, H. Majumdar, K. Ramachandran, and A. Shrivastava, *Nucl. Phys. A* **802**, 67 (2008).
- [45] M. J. Rhoades-Brown and P. Braun-Munzinger, *Phys. Lett. B* **136**, 19 (1984).
- [46] B. Pritychenko, J. Choquette, M. Horoi, B. Karamy, and B. Singh, *At. Data Nucl. Data Tables* **98**, 798 (2012).
- [47] S. Cohen and D. Kurath, *Nucl. Phys. A* **101**, 1 (1967).
- [48] Jenny Lee, M. B. Tsang, W. G. Lynch, M. Horoi, and S. C. Su, *Phys. Rev. C* **79**, 054611 (2009).
- [49] D. D. Armstrong, A. G. Blair, and H. C. Thomas, *Phys. Rev.* **155**, 1254 (1967).